Digital holography of particles: benefits of the "inverse problem" approach

Jérôme Gire, Loïc Denis, Corinne Fournier, Éric Thiébaut, Ferreol Soulez, Christophe Ducottet

Digital holography of particles: benefits of the "inverse problem" approach

J Gire[1,2,4], L Denis[1,3], C Fournier[1,4], E Thiébaut[2], F Soulez[1,2], C Ducottet[1,4]

[1] Laboratoire Hubert Curien (ex-LTSI) ; CNRS, UMR5516 ; Université Jean Monnet; 18 rue Pr Benoît Lauras, F-42000 Saint-Etienne, France
[2] Université de Lyon, Lyon, F-69000, France ; Université Lyon 1, Villeurbanne, F-69622, France ; Centre de Recherche Astronomique de Lyon, Observatoire de Lyon, 9 avenue Charles André, Saint-Genis Laval cedex, F-69561, France ; CNRS, UMR 5574 ; Ecole Normale Supérieure de Lyon, Lyon, France
[3] Ecole Supérieure de Chimie Physique Electronique de Lyon, 43 bd du 11 Novembre 1918, F-69616 Villeurbanne, France
[4] Institut Supérieur des Techniques Avancées de Saint-Etienne, Saint-Etienne, France

E-mail: `jerome.gire@univ-st-etienne.fr`

Abstract. The potential of in-line digital holography to locate and measure the size of particles distributed throughout a volume (in one shot) has been established. These measurements are fundamental for the study of particle trajectories in fluid flow. The most important issues in digital holography today are: the poor depth positioning accuracy, the transverse field of view limitation, border artifacts and the computational burden. We recently suggested an "inverse problem" approach to address some of these issues for the processing of particle digital holograms. The described algorithm improves axial positioning accuracy, gives particle diameters with sub-micrometer accuracy, eliminates border effects and increases the size of the studied volume. This approach for processing particle holograms pushes back some classical constraints. For example, the Nyquist criterion is no longer a restriction for the recording step and the studied volume is no longer confined to the field of view delimited by the sensor borders. In this paper we present a review of limitations commonly found in digital holography. We then discuss the benefits of the "inverse problem" approach and the influence of some experimental parameters in this framework.

PACS numbers: 07.05.P, 42.40, 06.30.G

Keywords: digital holography; in-line holography; inverse problem; ghost images; border effects; signal to noise ratio;

Submitted to: *Meas. Sci. Technol.*

1. Introduction

Digital in-line holography is a 3D imaging technique which has been widely developed during the past decades. This technique achieves the 3D reconstruction of volume objects from a 2D image and reaches accuracies in the range of - or smaller than - the wavelength [1, 2, 3]. Digital holography can solve two types of problems: (P1) the 3D reconstruction of object surfaces (P2) the 3D localization of micro objects spread throughout a volume.

Advances made in fluid mechanics, especially in digital methods make simulations of complex flows possible and generate a real need for experimental techniques which can analyze 3D flows. In this context, digital holography is one of the best suited techniques for the tracking of particles throughout a volume (P2). It has been demonstrated that in-line holography (see figure 1) is adapted to this kind of problem [4, 5], in particular thanks to its insensitivity to vibration and thanks to the simplicity of its setup.

Past few years, numerous algorithms for analysis of micro-particle holograms have been proposed (see for example research contributions in special issues [2, 6]). They are mostly based on a common approach for hologram processing (hereafter denoted as the classical approach): digital reconstruction based on the simulation of the hologram diffraction. They suffer from artifacts intrinsic to holography: twin-image contamination of the reconstructed images, image distortions for particles located close to the hologram borders. The analysis of the reconstructed planes is therefore penalized by these defects. In contrast with this approach, the inverse problem perspective does not transform the hologram and performs particle detection by matching a model of the hologram. This technique extracts more information from the hologram and solves two essential problems in particle digital holography: the improvement of the axial localization accuracy of a particle and the enlargement of the studied field beyond the physical limit of the sensor size. The drawbacks of this approach is a computation load heavier than that of the classical techniques, especially in the case of a large number of particles and this approach is also restricted to particles modeled by few geometrical parameters.

We have recently described this novel approach and proved its feasibility to process experimental holograms of water droplets [7, 8]. We propose in this paper to study the benefits of the "inverse problem" approach. For that purpose, in section 2, we introduce a review of the classical approach for hologram 3D reconstruction. Its drawbacks are summed up and constraints on the experimental setup revisited. In section 3, we recall the principle of the approach based on "inverse problem" and introduce some mathematical notations. Finally we discuss in section 4 benefits of the "inverse problem" approach in the light of the new influence of some experimental parameters. We explain why the Nyquist criterion is no longer a restriction and why the pixel integration has to be taken into account. We also analyze the benefit of the cleaning step to the signal to noise ratio.

2. Hologram-diffraction based approaches and their limitations

In this section, we summarize hologram diffraction-based approaches used in in-line particle holography and their limitations. We then present, in more detail, some of their drawbacks and point out some of the work in the literature that describe them.

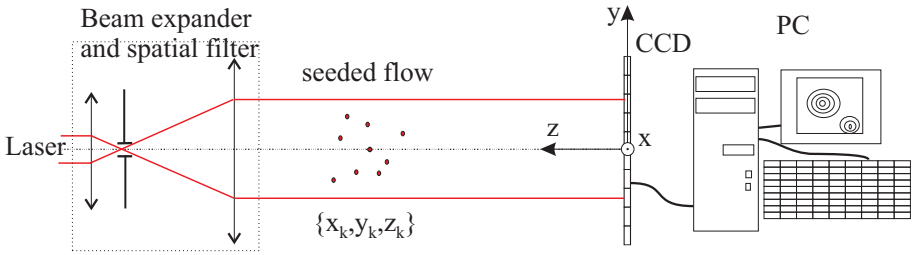

Figure 1. The in-line holography setup

2.1. Presentation of these methods

The classical 3D reconstruction of digital holograms is performed in two steps. The first step is based on a numerical simulation of the optical reconstruction. A whole volume is obtained by computing the diffracted field in planes located at increasing distances from the hologram (see figure 2). Different techniques to simulate diffraction under Fresnel approximation have been used (Fresnel transform [9], Fractional Fourier Transform [10, 11] or wavelets transform [12, 13]). The second step consists in localizing and sizing each particle in the obtained 3D image. The best focusing plane for each particle has to be detected. Various criteria are suggested in the literature. Some are based on the local analysis of the gray level of the reconstructed volume. For example, one searches for the minimum of the gray level on the z-axis crossing the particle center [14] or computes the barycenter of the labeled particle image after thresholding of the 3D reconstructed image [15]. Some authors use the imaginary part of the reconstructed field [16]. Other approaches are based on an analysis of the object's 3D image. Liebling uses the criterion of the sparsity of wavelets coefficients [17]; and Dubois uses the minimization of the integrated reconstructed amplitude [18]. Hologram-diffraction based approaches, can suffer from various limitations:

(i) the depth accuracy is weak (section 2.3);
(ii) the field of view is limited and, in practice, must be restricted to the center of the reconstructed images to reduce the border effects (section 2.4);
(iii) spurious twin-images of the particles get reconstructed;
(iv) multiple focusing can occur around the actual depth location of each particle [19];
(v) under-sampled holograms can lead to ghost images (section 2.2);
(vi) algorithms of this approach are often time-consuming (section 2.5);
(vii) the analysis of reconstructed planes is possible only for low concentrated holograms.

We recall in the next subsections some of these limitations.

2.2. Ghost images

Due to technological constraints, digital holography suffers from the bad resolution of digital cameras (about 50 times worse than holographic plates). For a correct sampling of the image, the maximal frequency is imposed by the pixel sampling ($\Delta\xi$). When the Nyquist criterion is not fulfilled (signal frequency higher than the Nyquist frequency), an aliasing phenomenon appears. In the in-line holography case, where the recorded

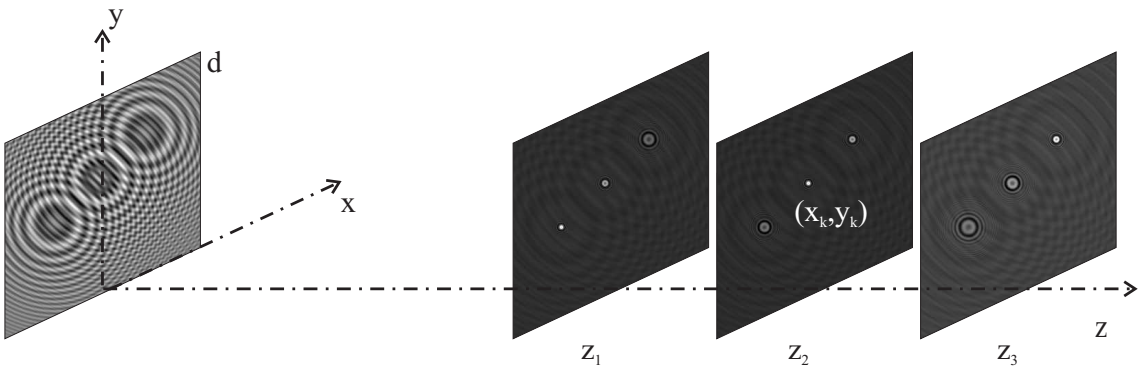

Figure 2. Reconstruction illustration.

signal is a convolution of the aperture of the object by a 2D chirp function (Fresnel function), aliasing produces ghost images in the reconstructed images [20, 21, 22, 23]. These ghost images can lead to false detections. In most cases the windowing of the Fresnel function by the diffraction envelope of the particle (defined as $J_{1c}(x) = J_1(x)/x$ where J_1 is the Bessel function of the first order) reduces ghost images amplitude to below that of the true image. Nevertheless, these ghost images can be mistaken for small particles in a classical approach.

Some solutions have been proposed to overcome this problem. Onural and Stern [21, 23] suggest a filtering of these ghost images in the reconstructed planes (in the case of known location of the "true" particle). Jacquot [20] presents an over-sampling of the hologram and Coupland [22] suggests removing ghost images by using an irregular sampling of the signal, which involves a decrease of the amplitude of these images compared to the real ones. Let us notice that these last two methods require some heavier experimental setups.

To avoid ghost image occurrence in the hologram, the Nyquist criterion must be respected. For a particle located on the optical axis at a distance z from the hologram, the following inequality must be satisfied [5]:

$$z > z_{\min} = \frac{L\,\Delta\xi}{\lambda} \tag{1}$$

where L is the width of the sensor and λ is the laser wavelength. This imposes either to use a high resolution sensor (small $\Delta\xi$) or have the particles at a distance greater than $z_{\min}$. For a given pixel size, the camera cannot be positioned too close to the particles. This may result in excessive blurring of the interference fringes (their contrast decreases when the camera-particles distance increases).

2.3. Accuracy

In optics, the resolution is defined by the Rayleigh criterion as the minimum separation distance between two points - located at a given distance from the imaging system - to be spatially resolved [24]. In the case of an optical system containing a square aperture, and under the Fresnel approximation, two points that are located close to the optical axis are imaged distinctly, when the center of the sinc function generated by a point corresponds exactly to the first zero of the sinc function generated by the

second point. Under this condition, the lateral resolution δx of an imaging system of aperture L is given by:

$$\delta x = \frac{\lambda z}{L} \tag{2}$$

where z corresponds to the distance aperture - image plane. In the same way, the axial resolution is closely linked to the depth of the 3D reconstructed images. The z-resolution of an imaging system is given [25] by:

$$\delta z = \frac{\lambda z^2}{L^2} \tag{3}$$

Let us notice that in digital holography of particles, the recording model of a hologram (see section 3.1) is not valid when particles are close to each other (the interferences between particles as well as the reference wave distortion are not negligible). However this case is unlikely in digital holography of particles (the number of particles is limited by the Royer criterion [26]). Rayleigh criterion is therefore not the most discerning to define the accuracy in digital holography particle tracking velocimetry, which is a detection problem rather than an imaging problem.

The accuracy is more relevantly defined as a statistical measure of the difference between the true value and its measure (typically the standard deviation of the error for unbiased measure). The accuracy of the measure depends on the depth of field, but can be many times fainter. It depends also on the sensor definition, the quantization, the particles concentration as well as the transverse location of the particles. The last point is a consequence of the borders artifacts (generated by the classical reconstruction, see section 2.1) which worsens the measured accuracy. This multi-parameter dependency explains why accuracy in digital holography is always given according to experimental settings [16, 14, 27, 28, 29, 30].

2.4. Border effects

A drawback which can prove embarrassing within the framework of metrology is the appearance of some artifacts in the reconstructed 3D image due to hologram truncation. This problem is all the more important since digital camera sensors are small compared to holographic plates (their surface is a hundred times less). In holography, the signal of each particle is spread over a large surface. The loss of the fringes outside of the sensor is at the origin of the artifacts named "border effects". This phenomenon distorts the particle reconstruction in the 3D space and so generates errors in the positioning and the estimation of the particles' diameters. This phenomenon is illustrated in figure 3. This figure shows the distortion of a particle located on the border of an experimental hologram of water droplets on several consecutive reconstructed planes (see section 3.4 for experimental setup description).

Hologram diffraction-based techniques require an expansion of the hologram outside its boundaries. The hologram can either be zero-padded, periodized or mirror-extended. In each case, the recorded fringes are completed by erroneous values outside the hologram. This leads to distorted and low-contrasted 3D images in the reconstructed planes (figure 3). These artifacts, generating a loss of accuracy in the 3D reconstruction, restrict the usability of these reconstruction approaches to the area located in the center of the hologram (where interference patterns are slightly truncated). Several methods have been proposed to reduce the border effects. Dubois suggested a technique to extend the hologram so as to suppress the truncation effect

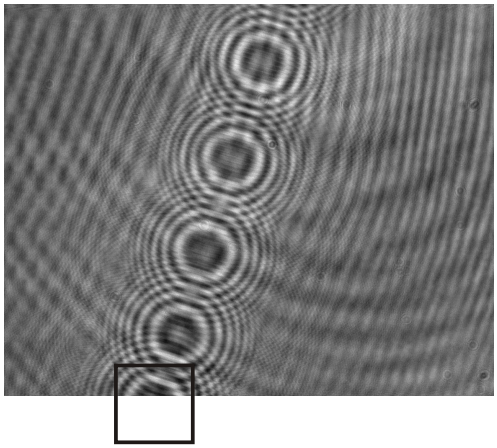

(a)

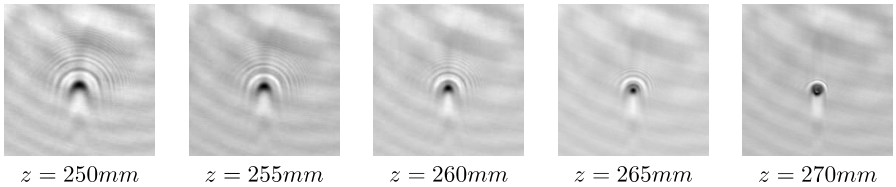

(b)

Figure 3. Illustration of artifacts appearing during the numerical reconstruction due to the truncation of diffraction rings on the hologram border: (a) experimental hologram of droplets (b) numerical reconstructions at different depths z. The images represented in (b) correspond to the square area drawn on the hologram (a).

on the border [31]. Cuche proposed a windowing method based on a weighting of the hologram border by a cubic spline. This allows for the reduction of the border effects in the central part of the field of view, at the cost of a loss of contrast close to the borders [32]. These methods improve the field border reconstruction but do not facilitate accurate out-of-field detections.

2.5. Computation complexity

The processing time is often a limiting factor in the implementation of algorithms as many applications require a real-time processing. In digital holography, heavy computations are necessary and hologram analysis is, therefore, often postponed. When temporal series of holograms are considered, the computational load becomes very heavy. Within the framework of classical 3D reconstruction, the processing time depends on the 3D image reconstruction step and the segmentation step. The 3D image reconstruction can be performed by computing one 2D-FFT (Fast Fourier Transform) for each depth. As we saw in section 2.1, the segmentation step can be realized via numerous algorithms. So the complexity of this part can be more or less important and can depend on many parameters (complexity of algorithm used, image size, number of particles, ...) according to the chosen method. The complexity of hologram processing, bounded by that of the 3D reconstruction step, remains time-consuming for an industrial framework use. Recently, some solutions as parallel computing [33] or even some implementations in dedicated circuits as FPGA (Field-Programmable Gate Array) [34] have been proposed in order to reduce this problem. Direct processing approaches that do not require 3D reconstruction were also suggested to quickly extract the mean particle size [35] or the distribution of directions of fibres [36].

3. Review of the "inverse problem" approach

In this section we review a method based on an "inverse problem" approach for digital hologram analysis. We first describe the recording model of the hologram which is used in this method and introduce mathematical notations used in section 4. Then we review the "inverse problem" approach and the iterative algorithm used to setup this approach. Finally we sum up the main benefits of this approach.

3.1. Recording model of the hologram

We consider an in-line holographic setup (see figure 1) where studied particles are illuminated by the laser beam and both reference wave and object wave interfere and are recorded by the camera. In this section we describe the model of the hologram under Fresnel's diffraction approximation for spherical particles. This model is the basis for our "inverse problem" approach. The resulting hologram expression is a sum of terms depending on the location and size of each particle. In the case of digital holography of spherical micro-particles, each particle is described by few parameters $\{x_k, y_k, z_k, r_k\}$: x, y, z represent the spatial coordinates and r the radius. The notations and coordinate system we use are summarized in figure 4. The simplified model of hologram intensity measured by the detector can be written as follows [8]:

$$I(x,y) = I_0 - \sum_{k=1}^{n} \alpha_k \, g_k(x - x_k, y - y_k) + I_{bg}(x,y) \tag{4}$$

where α_k is an amplitude factor of the diffraction pattern of the k-th particle, I_0 represents the incident intensity on the sensor and I_{bg} the background noise. The function $g_k(x,y)$ represents the diffraction pattern of one particle and is given by the

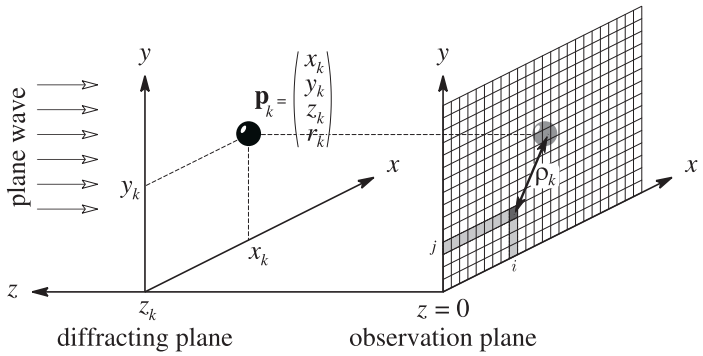

Figure 4. Notations used in the hologram model.

following equation:

$$g_k(x,y) = \frac{\pi\, r_k^2}{\lambda z_k}\; J_{1c}\left(\frac{2\pi\, r_k\sqrt{x^2+y^2}}{\lambda z_k}\right) \sin\left(\frac{\pi(x^2+y^2)}{\lambda z_k}\right) \tag{5}$$

where λ is the laser wavelength. Let us notice that the speckle noise (due to second order interference terms) is negligible compared to the amplitude of the diffraction patterns of the other particles (Meng [37]). We therefore neglect this noise. The background noise ($I_{bg}(x,y)$) comprises the noise due to experimental setup, due to the electronic noise and due to the quantization noise.

The detector is a matrix of size (N_i,N_j), thus the intensity is only known on discrete values (i,j). The recorded data (4) on the pixel $[i,j]$ are:

$$d[i,j] = I_0 - \sum_{k=1}^{n} \alpha_k\, g_k[i,j] + I_{bg}[i,j] \tag{6}$$

where $g_k[i,j] = g_k(x - x_k, y - y_k)$ with $x - x_k = i\Delta\xi$ and $y - y_k = j\Delta\xi$. This model of a hologram is an additive model: the hologram intensity consists of the sum of the diffraction-patterns of the n particles plus a remaining background noise I_{bg}.

3.2. Inverse problem formulation

We saw in section 2, the description of the classical approaches. These methods are based on the diffraction of the hologram. In the field of particle holography, hologram processing amounts to a detection problem for which the most relevant domain is that of signal processing. The reconstruction of a 3D image then appears unnecessary and the problem of particle detection can be reformulated as a problem of diffraction-pattern detection. The expression of the diffraction-pattern of a particle with given size and location is well-known and therefore easy to compute (direct problem) (see section 3.1). Let us consider a population of particles characterized by their parameters $\{x_k, y_k, z_k, r_k\}_{k=1,\ldots n}$. The 4D reconstruction of the set of particles (locations and sizes) that corresponds to a given hologram is a much more complex problem (inverse problem). The analysis of a particle hologram requires solving such an inverse problem [7, 8]. We recall in the following paragraph how the hologram analysis problem can be formulated as a minimization problem.

The experimental hologram $d[i,j]$ is modeled by a parametric model $m[i,j]$ based on a diffraction-pattern model (5) which depends on a set of parameters $\{x_k, y_k, z_k, r_k\}_{k=1,\dots n}$ corresponding to the location and size of each of the n particles:

$$m[i,j] = I_0 - \sum_{k=1}^{n} \alpha_k \, g_k[i,j] \tag{7}$$

The problem of particle detection can be expressed as a global optimization problem. It consists of finding the optimal set of parameters which minimizes the penalty function $\mathcal{P}$ of weighted least squares defined by:

$$\mathcal{P} = \sum_{i=1}^{N_i} \sum_{j=1}^{N_j} w[i,j] \left(m[i,j] - d[i,j]\right)^2 \tag{8}$$

where $w[i,j]$ is a weight matrix taking into account the truncation effect and possible dead pixels and can be defined as:

$$w[i,j] = \begin{cases} 1 & \text{if the pixel } (i,j) \text{ is measured,} \\ 0 & \text{otherwise.} \end{cases}$$

In the following section, we describe the iterative algorithm we suggested in reference [7]. It reaches the minimum of the penalty function $\mathcal{P}$ and therefore locates and sizes the particles recorded in the hologram.

3.3. Iterative particle detection

The algorithm performs the detection on a particle per particle basis. Parameter sets of the particles are obtained in an iterative manner by local optimization. At iteration ℓ, the parameters $\{x_\ell, y_\ell, z_\ell, r_\ell\}$ of the ℓ-th particle are determined by minimization of the weighted least-squares penalty function $\mathcal{P}_\ell$:

$$\mathcal{P}_\ell = \sum_{i=1}^{N_i} \sum_{j=1}^{N_j} w[i,j] \left(m_\ell[i,j] - d_\ell[i,j]\right)^2 \tag{9}$$

where $m_\ell[i,j]$ corresponds to the intensity contribution of the ℓ-th particle and $d_\ell[i,j]$ represents the centered residual data at the ℓ-th step. It can be detailed from equations (6) and (7) as follows:

$$d_\ell[i,j] = d[i,j] + \sum_{k=1}^{\ell-1} \alpha_k \, g_k[i,j] + a_\ell \tag{10}$$

where a_ℓ corresponds to the centering constant. Each iteration can be broken down into three steps:

- Global detection step
  The penalty function is sampled and the minimum gives a first estimate of the parameters $\{x_\ell, y_\ell, z_\ell, r_\ell\}$ of the ℓ-th particle [8].
- Local optimization step
  It is achieved by minimizing the penalty function $\mathcal{P}_\ell$ (9). The parameters $\{x_\ell, y_\ell, z_\ell, r_\ell\}$ are refined.
- Cleaning step
  The model of the ℓ-th particle of optimal parameters $\{x_\ell, y_\ell, z_\ell, r_\ell\}$ is subtracted from the hologram resulting in residual data.

Let us notice that the order of particle detection corresponds roughly to a decrease of particle energy. Let us call the energy of the ℓ-th particle signal the "particle energy" defined as: $\sum_{i=1}^{N_i}\sum_{j=1}^{N_j} w[i,j]\, m_\ell^2[i,j]$.

3.4. Main results

This approach removes some limitations of classical methods. Firstly, by expressing the detection problem directly in the hologram plane (8), we get rid of some artifacts that appear in holographic reconstruction (twin-image problem, multiple focusing). Secondly, due to the cleaning step, our algorithm is able to detect particles with faint energy. Thirdly, the truncation outside the borders of the hologram is modeled by the weight matrix. This suppresses the bias due to the truncation of diffraction rings. This is of interest value for fluid mechanics measurements as it allows to largely increase (from less than 1cm^2 to a few cm^2) the upper limit of the scale of observable phenomena. Finally, let us notice two drawbacks: this approach is limited (due to computational complexity) to simple particle models (i.e. parametric models depending on few variables) and is more time consuming than the classical approaches. The computational burden of our algorithm is greater than for most classical approaches as it requires as many volumetric reconstructions (based on 2D-FFT) as the number of detected particles [8]. The computation time of the 2D-FFT depends on the hologram size; and for out-of-field particles detection, the size of the hologram has to be strongly increased as can be seen in figure 5.

These results have been validated on both simulated and real data [7, 8]. Figure 5 shows the results of the processing of one experimental hologram (1024×1024, pixel size of $6.7\mu m \times 6.7\mu m$, wavelength of $0.532\mu m$) of water droplets (diameter of $90\mu m$) injected by a piezoelectric injector located at 250mm from the sensor (figure 3). We can see in figure 5a, in the center, the camera sensor field which contains hologram data. It should be noted that only four particles have projections located on the sensor, while the whole image represents the studied field of view where 16 particles can be located. This means that the surface of the effective field of view has been increased by a factor of 16 compared to the sensor surface. The figure 5b displays a 3D reconstruction of 200 holograms. These results show that the algorithm is insensitive to the experimental noise. A study of the accuracy for the location and size estimation of particles has been realized on simulations (using parameters comparable to the experimental ones). It shows that the accuracy has been greatly improved. The transverse location (x y) has a standard deviation of 1/20 pixel ($0.3\mu m$) and does not depend on the particles' location. The accuracy along the depth direction has a standard deviation of 1/7 pixel ($0.9\mu m$); that is much better than the optical resolution in the experimental conditions. It becomes comparable to the transverse accuracy. The estimation of the diameter has also been improved (standard deviation of $0.4\mu m$).

4. Benefits of the "inverse problem" approach

The parameters of the experimental setups have to fulfill different influences on 3D reconstruction depending on the method used for hologram analysis. In this part, we compare the influence of recording parameters in the classical approach with their influence in the "inverse problem" approach. We discuss the classical limitation on the

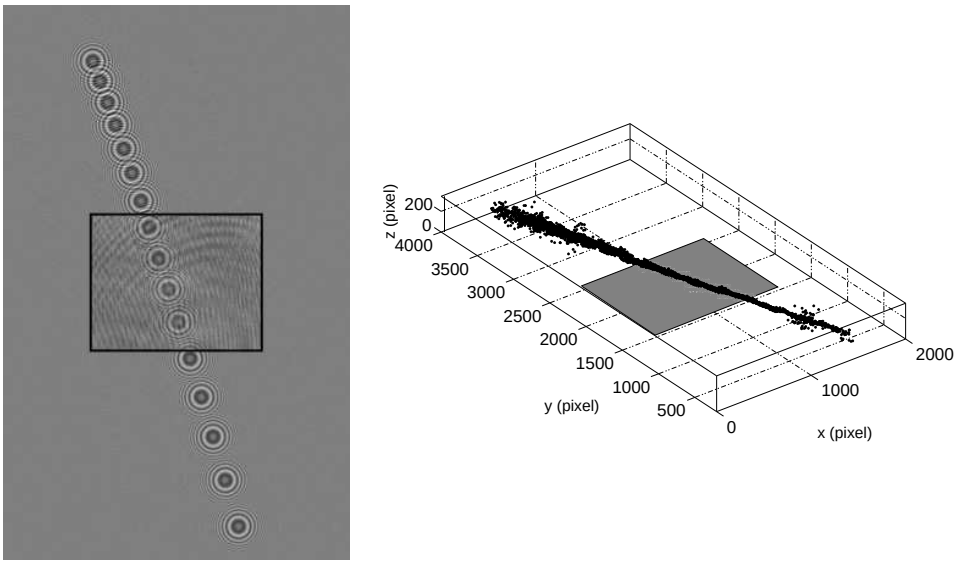

(a) (b)

Figure 5. Illustration of droplets detection located out-of-field: (a) superimposition of one hologram of the series and the model of this hologram calculated from 16 detected particles (including 12 out-of-field); (b) represents the 3D jet flow obtained by detecting all particles located in a field corresponding to more than 16 times the hologram surface. The surface corresponding of the sensor is represented in gray. The droplets detection is realized without significant bias even for particles located far away from the sensor.

recording distance imposed by Nyquist criterion and show that the low-pass filtering effect due to the fill-factor is no longer negligible in our approach. Finally, we analyze the signal to noise ratio of a particle in the hologram and investigate the improvement brought by the cleaning procedure.

4.1. Ghost images

The diffraction-pattern is composed of two main terms: the frequency modulation (included in sin function) and the amplitude modulation (included in J_{1c} function). This amplitude modulation of the signal decreases the energy of ghost images which could be mistaken for small particles in a classical approach (section 2.2).

In the "inverse problem" framework, ghost images are less of a problem for two reasons. First, we search the best fit between the hologram pattern and a model of the diffraction pattern which is sampled in the same way and thus contains the same aliasing artifacts (ghost images). Secondly, at the cleaning step, the whole pattern (ghost images) is subtracted from the hologram. Furthermore, the order in which the particles are removed corresponds to a decrease of the particle energy, and a ghost image should thus not be detected before its real image is detected.

However, to get it work, the envelope of the J_{1c} has to decrease the energy of ghost images in a significant way. The decrease depends on the $J_{1c}\left(\frac{2\pi\, r\, \rho}{\lambda z}\right)$ function (where $\rho = \sqrt{x^2 + y^2}$). The center of the first ghost image is located where the frequency (of

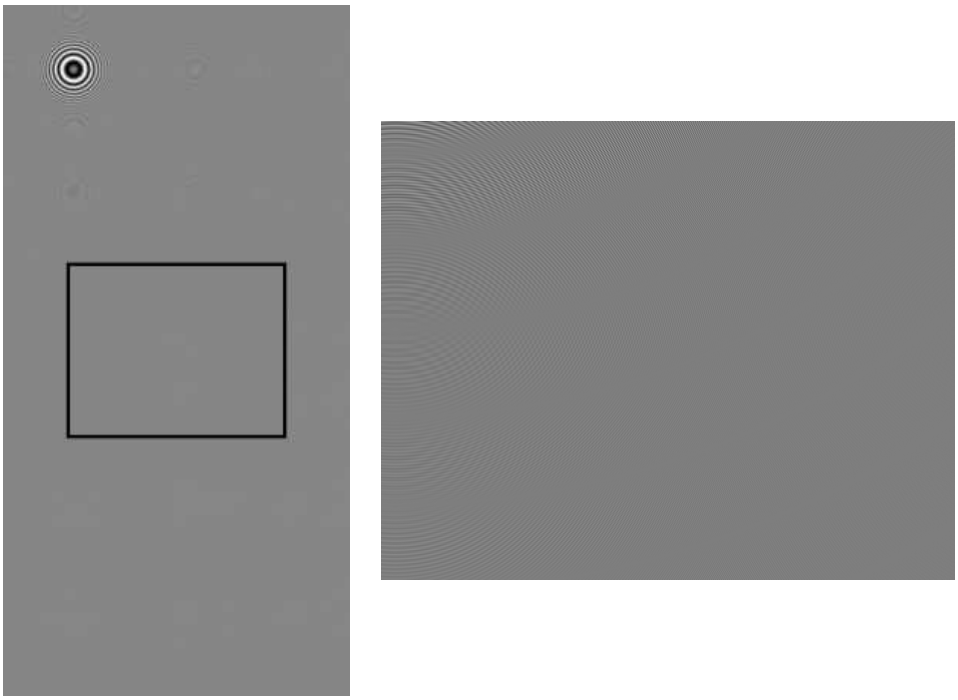

(a) (b)

Figure 6. (a) Simulation of a hologram of one "out-of-field" particle. The rectangle corresponds to the numerical sensor limits. (b) Zoom on the sensor area (the visualization dynamics has been enhanced).

the sinc function) is equal to twice the Nyquist frequency: $\frac{\rho}{\lambda z} = \frac{1}{\Delta\xi}$. The decrease of the ghost image in it center is thus: $J_{1c}\left(\frac{2\pi\, r}{\Delta\xi}\right)$. For a decrease greater than 20%, the following inequality has to be satisfied: $\frac{2r}{\Delta\xi} > 0.42$. In most experimental cases, the particle diameter is larger than the width of the pixel sensitive area, then the signal amplitude of ghost images is much lower than that of the real image. The ghost images cannot thus be mistaken for real particles.

In the experimental results summarized in 3.4 (see figure 5) where $\frac{2r}{\Delta\xi} \simeq 13$, 1560 particles patterns (out of 3000 detected particles) do not fulfill the Nyquist criterion. An illustration of this phenomenon is given in figure 6. Figure 6a shows the hologram simulation of one out-of-field particle. The rectangle corresponds to the numerical sensor limits. A magnified image of the sensor part is presented in figure 6b with a gray level dynamic chosen so as to enhance the modulation of the signal. Moiré patterns can be seen in figure 6b.

In conclusion, the aliasing phenomenon may occur. As the sampling used for the model is the same as that of the experimental hologram, Moiré patterns can be considered as part of the signal. They are removed at the cleaning step. Note that the pixel integration must then be taken into account as shown in the next paragraph.

4.2. Pixel integration

An important parameter for digital sensors is the fill-factor that characterizes the effect of pixel integration. It is defined by the ratio of the sensitive surface to the pixel surface. Depending on the technology used (CCD or CMOS with or without micro-lenses) the fill factor may vary in large proportions. Each pixel of the sensor acts as a low-pass filter on the signal. This filter depends on the pixel size and on the fill factor. Under the hypothesis of small particles and square pixels, the recorded hologram expression given in equation (5) becomes [38]:

$$g_k(x,y) = \frac{\pi\, r_k^2}{\lambda z}\, J_{1c}\left(\frac{2\pi\, r_k \sqrt{x^2+y^2}}{\lambda z_k}\right) \sin\left(\frac{\pi(x^2+y^2)}{\lambda z_k}\right) \mathrm{sinc}\left(\frac{\pi\,\kappa\,\Delta\xi\, x}{\lambda z_k}\right) \\ .\ \mathrm{sinc}\left(\frac{\pi\,\kappa\,\Delta\xi\, y}{\lambda z_k}\right) \tag{11}$$

where sinc is represented by $\mathrm{sinc}\,(x) = \sin(x)/x$ and where κ corresponds to the ratio of the width of the sensitive surface to the width of the total pixel surface (κ^2 corresponds to the fill factor) and $\Delta\xi$ represents the pixel size.

As shown in equation (11), the signal is windowed by a sinc function. Its first zero is located at a distance $d = \frac{\lambda z_k}{\kappa \Delta\xi}$ from the center of the diffraction pattern. For a particle located in the classical field (restricted by the sensor size), the first zero is always located beyond the sensor borders when the Nyquist criterion is fulfilled ($z > z_{\min}$). For a particle located on the optical axis for $z = z_{\min}$ and $\kappa = 1$, the magnitude of the signal is reduced by ($1 - \mathrm{sinc}(\pi/2) \simeq 36\%$) by the sinc function on the sensor borders. The pixel integration is thus ignored in classical approaches [38].

In our approach the field of view size is no longer restricted to the size of the sensor. Besides, as we saw in section 4.1, the Nyquist criterion is no longer a constraint. These two associated facts make the pixel integration no longer negligible. The sinc function due to pixel integration has two effects: (1) it produces a decrease in the signal amplitude in the recorded high frequencies (this reduces the energy of the recorded particles especially for out-of-field ones) and (2) it changes the shape of the particle model. If this effect is not taken into account, the modeling errors can result in false detections. These two effects are discussed in the following paragraphs.

Figure 7a shows the sinc function (with parameters: $z = z_{\min}$ and $\kappa = 0.5$) for a particle located on the border of a field of view two times larger ($2L$) than the hologram size (L). The bright part represents the low energy attenuation ($1 - \mathrm{sinc}(\pi/4) \simeq 10\%$) and conversely the dark part corresponds to high energy attenuation ($1 - \mathrm{sinc}(3\pi/4) \simeq 70\%$). Figure 7b represents a line profile along the dash-dotted line in figure 7a. The vertical lines define the sensor boundaries. That shows that contrary to in-field particles, the reduction due to pixel integration cannot be ignored for out-of-field particles.

The distortion due to the sinc function is comparable to that of the J_{1c} function. More precisely, the fill factor effect becomes comparable when the first zero of the sinc function function is close to the first zero of the J_{1c} function. Hence, we can establish the following relationship between the fill factor and the diameter of the particles when both have a similar influence. The first zero ($x_{J_{1c}}$) of the J_{1c} function is:

$$x_{J_{1c}} = \frac{1.22\,\lambda\, z}{2r}, \tag{12}$$

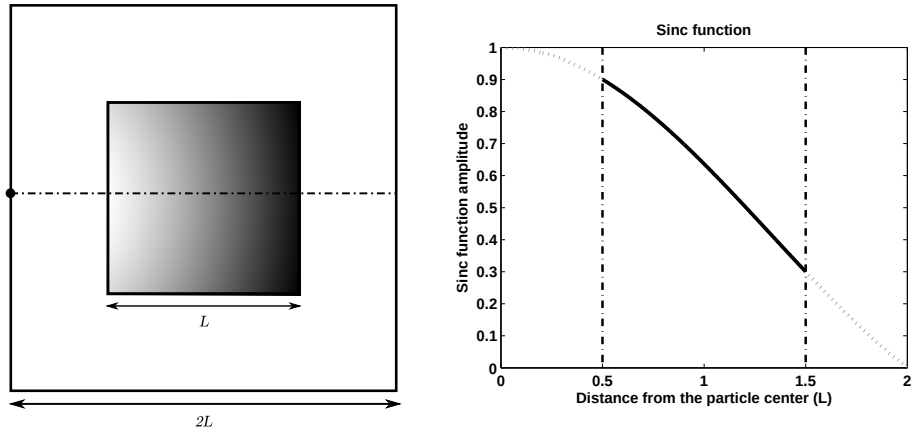

(a) (b)

Figure 7. (a) Sinc function generated by the pixel integration, simulated for $z = z_{\min}$ (respect with the Nyquist criterion) and $\kappa = 0.5$. It shows the shape deformation and decrease of the signal amplitude for a particle located out-of-field (on the borders of a field of view two times larger the sensor). Low reduction is represented in white and high reduction in black. (b) Line profile along the dotted line on figure (a). Sensor borders are represented by vertical lines.

whereas the first zero (x_{sinc}) of the sinc function is:

$$x_{\text{sinc}} = \frac{\lambda\, z}{\kappa\, \Delta\xi}. \tag{13}$$

And because we consider $x_{\text{J}_{1c}} = x_{\text{sinc}}$, combining (12) and (13) leads to:

$$2r = 1.22\kappa\, \Delta\xi. \tag{14}$$

If the particle diameter is lower than or close to the width of the pixel sensitive area, the pixel integration effect is as important as the J_{1c} function effect. **Thus, if $2r \gg 1.22\kappa\, \Delta\xi$ the effect of the integration over the pixel has little influence compared to the J_{1c} function effect. Otherwise the pixel integration effect is no longer negligible and can thus induce an error on the measurement of the particle diameter.** Indeed, during the detection step, the diameter is estimated thanks to the amplitude modulation (due to the diffraction envelope of the particle (J_{1c})). The pixel integration which modifies this amplitude modulation can thus bias the measurement of the particle diameter.

We can reduce the effect of the pixel integration by taking it into account in our model. That will take the shape distortion into account but the loss of information due to the reduction of the signal dynamics and the quantization problem will remain.

4.3. Signal to noise ratio in the hologram

Noise is a major problem in holography. It has been studied by some authors [26, 37]. A hologram is exploitable if the recorded signal of a given particle is high enough with respect to the noise. In this section, we propose to study the signal to noise ratio (SNR) in the hologram with and without cleaning. For that purpose we choose to work in the hologram data. Thus we define a SNR measuring the relative influence

of the signal of a given particle in the hologram with respect to the surrounding noise on this hologram. Other definitions of the SNR can be proposed (for example in the reconstruction plane) in order to take into account the particle detection process but we prefer in this study to use a simpler approach independent of the detection and/or reconstruction used. In this approach, we consider that the noise can be broken down into two components: (1) the sum of the signal of each particle and (2) the background noise defined in section 3.1.

4.3.1. Definition of the signal to noise ratio in the hologram Without a cleaning step, the signal amplitude of particles decreases according to the distance from the particle to the hologram center, while the noise level remains constant. The SNR therefore decreases according to the transverse distance. In our approach, the cleaning effect on the noise has to be taken into account. Actually, the noise level decreases as particles are removed. Nevertheless the signal amplitude of particles also decreases according to the distance from the particle to the hologram center, especially for particles located close to the border or out-of-field.

To quantitatively study this SNR level in hologram analysis, we define it as the ratio of the variance of the ℓ-th particle signal to the variance of the two noise terms. Let us write the hologram d_ℓ (10) as a sum of the diffraction pattern of the ℓ-th particle $C_{s\ell}$, the other diffraction patterns $C_{p\ell}$, and the background noise C_{bg}:

$$d_\ell[i,j] = I_0 - \underbrace{\alpha_\ell\, g_\ell[i,j]}_{C_{s\ell}(i,j)} - \underbrace{\left(\sum_{k=\ell+1}^{n} \alpha_k\, g_k[i,j]\right)}_{C_{p\ell}(i,j)} + \underbrace{I_{bg}[i,j] + a_\ell}_{C_{bg}(i,j)} \tag{15}$$

Note that the noise term $C_{p\ell}$ has the same spectrum as the signal $C_{s\ell}$ and is therefore not reduced in our match-filter detection approach. As the two noise term $C_{p\ell}$ and C_{bg} can be considered as independent, the signal to noise ratio can be defined as:

$$SNR_\ell = \frac{\mathrm{Var}[C_{s\ell}]}{\mathrm{Var}[C_{p\ell}] + \mathrm{Var}[C_{bg}]} \tag{16}$$

where $\mathrm{Var}[C_{s\ell}] = \dfrac{1}{N}\sum_{i,j}\left(C_{s\ell}(i,j) - \mathrm{E}(C_{s\ell})\right)^2$,

with $\mathrm{E}(C_{s\ell}) = \dfrac{1}{N}\sum_{i,j} C_{s\ell}(i,j)$,

where N is the number of pixels.

4.3.2. Study of the SNR in the hologram as a function of the iteration step In order to study the signal to noise ratio evolution in our algorithm, we simulated holograms and the iterative cleaning. To simplify the study, we consider particles with constant radius r_0. Particles are randomly distributed under a uniform probability law throughout a volume centered on the optical axis and located at the distance z_0. The hologram simulations (example in figure 8a) are realized with a sensor of 1024×1024 (pixels size of $6.7 \times 6.7 \mu m$) placed at about $z_0 = 250mm$ from the studied volume. Figure 8b illustrates the transverse distribution of 2000 particles (diameter of $100\mu m$) throughout the volume of $27.44 \times 27.44 \times 50mm$: 125 particles are located on the sensor (dark gray rectangle), 500 out-of-field particles are located on the white rectangle (4 times the sensor surface), and 1500 particles are located in the light gray

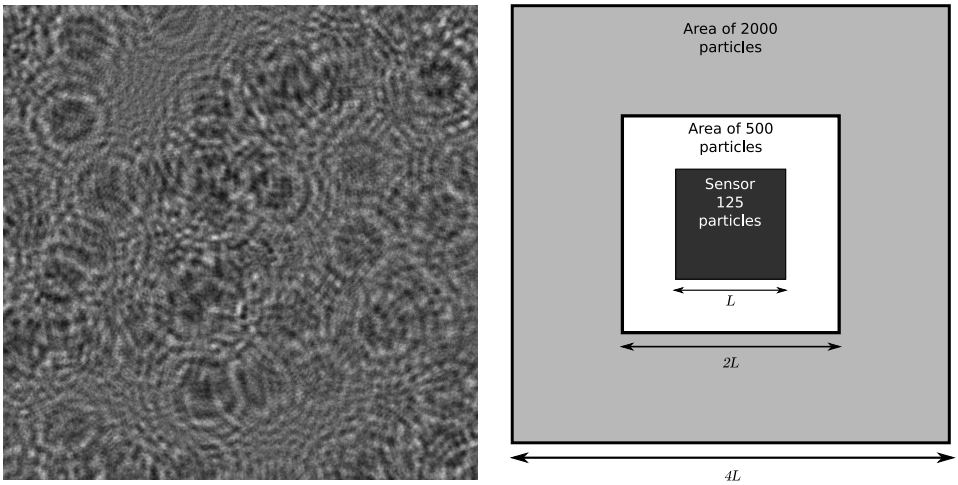

(a) (b)

Figure 8. (a) Example of a hologram simulation (1024×1024) made with 2000 particles (diameter of $100\mu m$) spread throughout a volume of $27.44 \times 27.44 \times 50mm$ located at $z0 = 250mm$. The pixel size is $6.7 \times 6.7\mu m$ and the laser wavelength is $0.532\mu m$. The hologram is coded on 8 bits depth. (b) Illustration of the distribution of particles throughout the volume: 125 particles are located on the sensor (dark gray area of width L), 500 out-of-field particles are located on the white area (4 times the sensor area), and 1500 particles are located around the white area (in the light gray part) which corresponds to the background noise.

part. These latter particles are not detected by our algorithm (since they are outside of the explored field of view). They therefore contribute to the noise. The light gray rectangle corresponds to the projected surface of the volume (16 times the sensor surface). The laser wavelength is $0.532\mu m$. Ten holograms (one of them shown in figure 8a) (8 bits depth) have been processed.

During the iterative process, particles are detected in decreasing order of energy. Let us notice that, in the case of mono-disperse particles, the ones of higher energy are located on the optical axis and that their energy decreases with the distance to the axis. We measure at iteration ℓ, the signal to noise ratio of the ℓ-th particle and represent (figure 9) its evolution as a function of the distance from the detected particle to the hologram border (negative for in-field particles, positive for out-of-field particles, the transition is represented by the vertical line). Figure 9(a,c) presents a comparison between signal to noise ratio variation in an approach without cleaning (plotted with $\times$) and in an iterative cleaning approach (plotted with $+$). Figure 9a shows the results obtained in one hologram while figure 9c displays a mean of the results obtained in 10 holograms. Let us notice that the dispersion observed in figure 9a is due to the sensor geometry (square); the diffraction patterns corresponding to a given distance from the border are not the same when the particle is located in a corner or on one edge. According to this figure 9a, it appears that as the distance to the nearest border increases (that means also the number of remaining particles decreases), the SNR increases as long as particles are located on the sensor. For out-of-field particles, the SNR sharply decreases. This decrease corresponds to the normal

decrease that we can notice on the curve of the SNR without removing particles. For out-of-field particles both curves have approximately the same evolution but are shifted up by an offset.

Figure 9b shows the ratio of the SNR of the approach using the cleaning compared to the SNR of the approach without cleaning (figure 9d shows a mean ratio computed over ten holograms). Let us notice that the SNR with the iterative cleaning is greatly improved compared to the SNR of the method without particle removal whatever the distance from the border (figure 9d). The SNR of out-of-field particles is greatly improved and the detection of these particles becomes easier. As a consequence, it is possible to increase the size of the field of view.

To conclude, we observe that the SNR in the hologram of the iterative cleaning method for out-of-field particles can be equivalent to the SNR of the approach without cleaning for particles located on the sensor. That allows an increase of the size of the allowed region of interest. And for out-of-field particles the signal to noise ratio decreases but is always largely higher in the conditions considered in the numerical simulations than the SNR without removing particles (see figure 9d). The influence of the background noise is presented in the following subsection.

4.3.3. Study of the SNR in the hologram as a function of noise level In this section, we study the effect of the cleaning as a function of noise level. The noise is generated by the 1500 particles located around the studied volume (see figure 8b) and by an additional white Gaussian noise with variance increasing from 0% to 25% of the hologram amplitude. This white noise corresponds to a background noise higher than the noise of the 1500 particles in the hologram. Simulations (figure 10a) are realized in a hologram generated with the same parameters of the example in figure 8a to which we add a Gaussian noise. The depth dynamic is adjusted as a function of the noise variance. Figure 10a shows the curves of the evolution of the SNR with respect to the iteration step in the case of the cleaning approach and for different levels of background noise. The cleaning has less effect when the background noise level is high (the curve with cleaning is almost like the curve without cleaning). In figure 10b, the SNR ratio is represented for each level of noise (ordinate axis in logarithmic scale). The benefit of the cleaning, though always present, decreases with growing noise levels. The increase of this ratio is mainly limited by the background noise. The ratio converges asymptotically to the value $(Var[C_{p0}] + Var[C_{bg}])/Var[C_{bg}]$. C_{p0} corresponds to the noise generated by all the particles. The convergence occurs when the variance of the particles becomes negligible compared to the variance of the background noise (usually when particles are far away from the optical axis - out of the sensor - and their energy is faint).

To conclude, the effect of the cleaning is limited by the background noise contained in the image. In the case of holograms with a high concentration of particles (with respect to the Royer criterion) and low background noise, the cleaning is efficient and provides a better measurement of particle parameters. Conversely the cleaning has less effect when the background noise level is high compared to the signal of the particles.

5. Conclusion

The "inverse problem" approach to particle hologram analysis introduced in [7, 8] improves detection accuracy, allows out-of-field particle detections and changes the

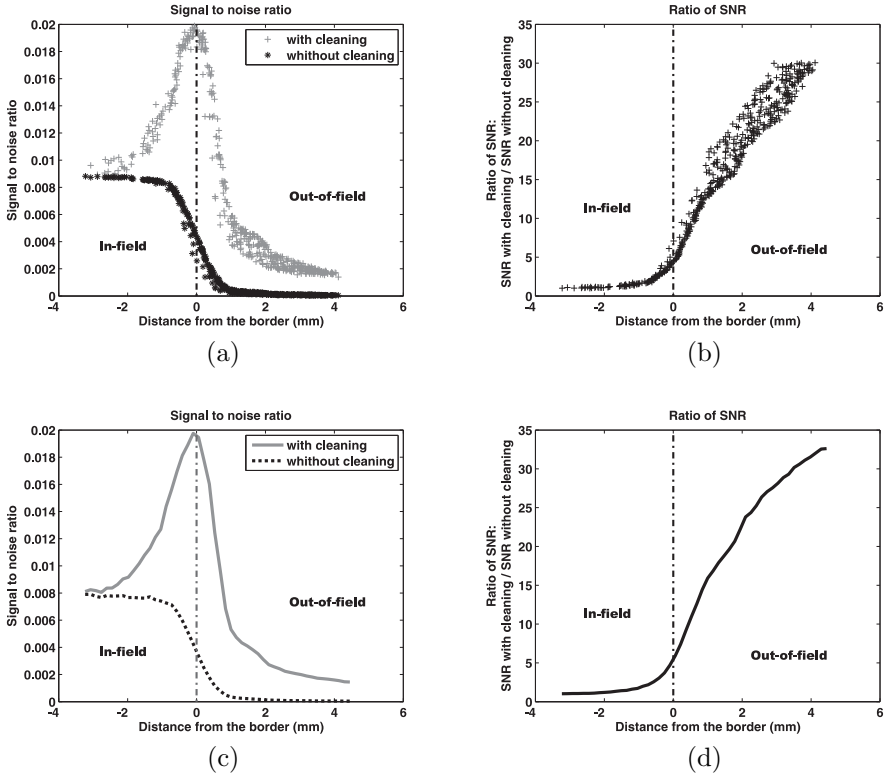

Figure 9. (a) Evolution of the SNR in the hologram during the detection of the particle. The curve plotted with × shows the evolution for an approach without particle cleaning. The curve plotted with + shows the evolution of the SNR for an approach with an iterative particle cleaning (described in section 3.3). (c) represents the mean curve of (a) over 10 simulations. (b) Ratio of the SNR of the iterative cleaning approach to the SNR without cleaning. (d) represents the mean curve of (b) over 10 simulations. The vertical dash-dotted line on all figures represents the transition between in-field and out-of-field particles.

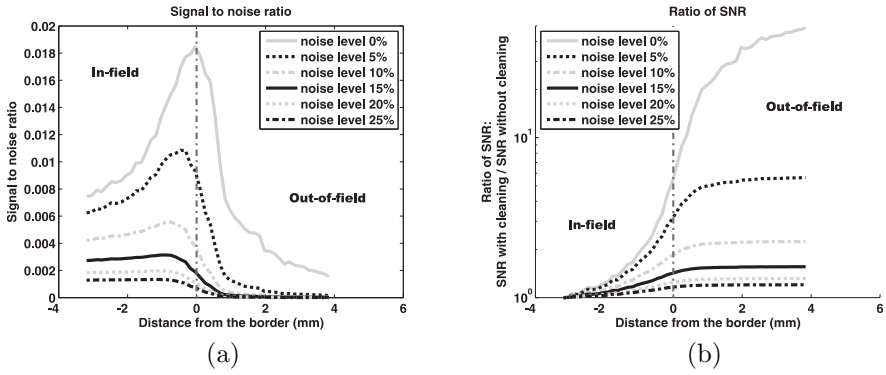

Figure 10. (a) Representation of the evolution of the SNR for the cleaning approach with different background noise level. (b) Ratio of the SNR of the iterative cleaning approach to the SNR without cleaning for the different curves plotted on (a). The vertical axis of this last curve is in logarithmic scale.

range of acceptable parameter settings. It modifies the classical constraints of digital holography of particles and suppresses spurious artifacts of the hologram diffraction approaches.

In this article, we show how the strongest limitations of the classical methods (aliasing which yields a minimal detection distance and edge effects which reduce the usable field of view) are removed by the "inverse problem" approach. Some experimental parameters as the fill factor have a negligible effect in the classical processing must however be taken into account.

Image processing is very often limited by the camera specifications and it is important to take into account two recording effects: the sampling phenomenon and the pixel integration. On the one hand, in the classical approach, the most limiting parameter is the signal sampling (Nyquist). The aliasing induced by signal under-sampling generates an aliasing phenomenon. In our case (see section 4.1), this phenomenon is less a constraint as it is possible to take it into account in our model (we can work over the Nyquist criterion). On the other hand, in the classical approach, the pixel integration has a small influence on the recording as the Nyquist criterion is a stronger limit. In our case, the pixel integration becomes important especially for out-of-field particles (see section 4.2). The low-pass filter due to pixel integration has two consequences: the distortion of the signal which can produce a loss of accuracy on the estimation of the particle sizes and the reduction of the signal magnitude on the sensor which reduces the SNR. Let us emphasize that the distortion phenomenon can be taken into account in the model in an "inverse problem" approach.

Finally, a study of the cleaning effect on the SNR (in the hologram) was carried out. The iterative cleaning improves the SNR of particles of faint energy (especially the ones that are located out-of-field). The background noise is a source of SNR degradation and can limit the capability to detect faint particles (i.e. small and/or out-of-field particles) and therefore can restrain the studied field. The detailed analysis of the detection limits achievable with the inverse problem approach is to be considered in further work.

References

[1] Marquet P, Rappaz B, Magistretti P J, Cuche E, Emery Y, Colomb T, and Depeursinge C. Digital holographic microscopy: a noninvasive contrast imaging technique allowing quantitative visualization of living cells with subwavelength axial accuracy. *Optics letters*, 30(5):468–470, 2005.

[2] Poon T C, Yatagai T, and Jüptner W. Digital holography – Coherent optics of the 21st century: introduction. *Applied Optics*, 45(5):821, 2006.

[3] Dubois F, Yourassowsky C, Monnom O, and Legros J-C. Digital holographic microscopy for the three-dimensional dynamic analysis of in vitro cancer cell migration. *Journal of Biomedical Optics*, 11(5):054032, 2006.

[4] Xu L, Peng X, Guo Z, Miao J, and Asundi A. Imaging analysis of digital holography. *Optics Express*, 13(7):2444–2452, 2005.

[5] Kreis T M. *Handbook of Holographic Interferometry, Optical and Digital Methods.* Wiley-VCH, Berlin, 2005.

[6] Hinsch K D and Herrmann S F. Special issue: Holographic particle image velocimetry. *Measurement Science & Technology*, 15(4), 2004.

[7] Soulez F, Denis L, Fournier C, Thiébaut E, and Goepfert C. Inverse problem approach for particle digital holography: accurate location based on local optimisation. *J. Opt. Soc. Am. A*, 24(4), 2007.

[8] Soulez F, Denis L, Thiébaut E, Fournier C, and Goepfert C. Inverse problem approach in particle digital holography : out-of-field particle detection made possible. *J. Opt. Soc. Am. A*, 24(12), 2007.

[9] Kreis T M, Adams M, and Jüptner W. Methods of digital holography : A comparison. In *SPIE97*, volume 3098, pages 224–233, 1997.

[10] Pellat-Finet P. Fresnel diffraction and the fractional-order fourier transform. *Optics Letters*, 19(18):1388–1390, 1994.

[11] Ozaktas H M, Arikan O, Kutay M A, and Bozdagt G. Digital computation of the fractional fourier transform. *Digital computation of the fractional Fourier transform. Signal Processing, IEEE Transactions on [see also Acoustics, Speech, and Signal Processing, IEEE Transactions on]*, 44(9):2141–2150, 1996.

[12] Buraga-Lefebvre C, Coëtmellec S, Lebrun D, and Özkul C. Application of wavelet transform to hologram analysis: three-dimensional location of particles. *Optics and Lasers in Engineering*, 33(6):409–421, 2000.

[13] Liebling M, Blu T, and Unser M. Fresnelets: New multiresolution wavelet bases for digital holography. *IEEE Transactions on image processing*, 12(1):29–43, 2003.

[14] Murata S and Yasuda N. Potential of digital holography in particle measurement. *Optics and Laser Technology*, 32(7 8):567–574, 2000.

[15] Malek M, Allano D, Coëtmellec S, Lebrun D, and Özkul C. Digital in-line holography for three-dimensional-two-components particle tracking velocimetry. *Measurement Science & Technology*, 15(4):699–705, 2004.

[16] Pan G and Meng H. Digital holography of particle fields: reconstruction by use of complex amplitude. *Applied Optics*, 42:827–833, 2003.

[17] Liebling M and Unser M. Autofocus for digital fresnel holograms by use of a fresnelet-sparsity criterion. *Journal of the Optical Society of America A*, 21(12):2424–2430, 2004.

[18] Dubois F, Schockaert C, Callens N, and Yourassowsky C. Focus plane detection criteria in digital holography microscopy by amplitude analysis. *Optics Express*, 14(13):5895–5908, 2006.

[19] Fournier C, Ducottet C, and Fournel T. Digital in-line holography: influence of the reconstruction function on the axial profile of a reconstructed particle image. *Measurement Science & Technology*, 15(4):686–693, 2004.

[20] Jacquot M and Sandoz P. Sampling of 2d images : prevention free from spectrum overlapping and ghost detection. *Optical Engineering*, 43(1):214–223, 2004.

[21] Onural L. Sampling of the diffraction field. *Applied Optics*, 39(32):5929–5935, 2000.

[22] Coupland J M. Holographic particle image velocimetry: signal recovery from under-sampled ccd data. *Measurement Science & Technology*, 15:711–717, 2004.

[23] Stern A and Javidi B. Analysis of pratical sampling and reconstruction from fresnel fields. *Optical Engineering*, 43(1):239–250, 2004.

[24] Goodman J W. *Introduction to Fourier Optics*. Mc Graw-Hill, 1996.

[25] Born M and Wolf E. *Principles of Optics*. Cambridge University Press, $7^{ème}$ edition, 1999.

[26] Royer H. An application of high-speed microholography: the metrology of fogs. *Nouvelle Revue d'Optique*, 5:87–93, 1974.

[27] Murata S and Hidaka N. Evaluation of the accuracy of the particle displacement measurement based on digital holography. In *The fifth JSME-KSME Fluids Engineering Conference*, pages 1–5, Nagoya, Japan, 2002.

[28] Malek M, Allano D, Coëtmellec S, and Lebrun D. Digital in-line holography: influence of the shadow density on particle field extraction. *Optics Express*, 12(10):2270–2279, 2004.

[29] Garcia-Sucerquia J, Xu W, and Kreuzer H J. Digital in-line holographic microscopy. *Applied Optics*, 45(5):836–850, 2006.

[30] Xu W, Jericho M H, Meinertzhagen I A, and Kreuzer H J. Digital in-line holography of microspheres. *Applied Optics*, 41:5367–5375, 2002.

[31] Dubois F Monnom O and Yourassowsky C. Border processing in digital holography by extension of the digital hologram and reduction of the higher spatial frequencies. *Applied Optics*, 41(14):2621–2626, 2002.

[32] Cuche E, Marquet P, and Depeursinge C. Aperture apodisation using cubic spline interpolation: application in digital holographic microscopy. *Optics communications*, 182(23):59–69, 2000.

[33] Satake S, Kanamori H, Kunugi T, Sato K, Ito T, and Yamamoto K. Parallel computing of a digital hologram and particle searching for microdigital-holographic particle-tracking velocimetry. *Applied Optics*, 46(4):538–543, 2007.

[34] Masuda N, Ito T, Kayama K, Kono H, Satake S, Kunugi T, and Sato K. Special purpose computer for digital holographic particle tracking velocimetry. *Optics Express*, 14(2):587–592, 2006.

[35] Denis L, Fournier C, Fournel T, Ducottet C, and Jeulin D. Direct extraction of the mean particle size from a digital hologram. *Applied Optics*, 45(5):944–952, 2006.

[36] Denis L, Fournel T, Fournier C, and Jeulin D. Reconstruction of the rose of directions from a

digital microhologram of fibres. *Journal of Microscopy*, 225(3):282–291, 2007.

[37] Meng H, Anderson W L, Hussain F, and Liu D D. Intrinsic speckle noise in in-line particle holography. *J. Opt. Soc. Am A*, 10(9):2046–2058, 1993.

[38] Kreis T M. Frequency analysis of digital holography with reconstruction by convolution. *Optical Engineering*, 41(8):1829–1839, 2002.